Journal of Sound and Vibration 406 (2017) 29–50

Contents lists available at ScienceDirect

Journal of Sound and Vibration

journal homepage: www.elsevier.com/locate/jsvi

A synergistic method for vibration suppression of an elevator mechatronic system

Bojan Z. Knezevic [a,*], Branko Blanusa [b], Darko P. Marcetic [c]

[a] Faculty of Mechanical Engineering Banja Luka, University in Banja Luka, Republic of Srpska, Bosnia and Herzegovina
[b] Faculty of Electrical Engineering Banja Luka, University in Banja Luka, Republic of Srpska, Bosnia and Herzegovina
[c] Faculty of Technical Sciences, University of Novi Sad, Republic of Serbia

ARTICLE INFO

Article history:
Received 23 July 2016
Received in revised form
5 May 2017
Accepted 5 June 2017

Keywords:
Elevator
Vibrations
Band-stop filter
Tuning algorithm
Jerk

ABSTRACT

Modern elevators are complex mechatronic systems which have to satisfy high performance in precision, safety and ride comfort. Each elevator mechatronic system (EMS) contains a mechanical subsystem which is characterized by its resonant frequency. In order to achieve high performance of the whole system, the control part of the EMS inevitably excites resonant circuits causing the occurrence of vibration. This paper proposes a synergistic solution based on the jerk control and the upgrade of the speed controller with a band-stop filter to restore lost ride comfort and speed control caused by vibration. The band-stop filter eliminates the resonant component from the speed controller spectra and jerk control provides operating of the speed controller in a linear mode as well as increased ride comfort. The original method for band-stop filter tuning based on Goertzel algorithm and Kiefer search algorithm is proposed in this paper. In order to generate the speed reference trajectory which can be defined by different shapes and amplitudes of jerk, a unique generalized model is proposed. The proposed algorithm is integrated in the power drive control algorithm and implemented on the digital signal processor. Through experimental verifications on a scale down prototype of the EMS it has been verified that only synergistic effect of controlling jerk and filtrating the reference torque can completely eliminate vibrations.

1. Introduction

Technological development and the development of construction activities enabled the construction of multi-storey buildings. Urbanization and the expansion of urban areas additionally motivated building construction, thus increasing density and concentration of population in urban cores. With the development of building construction elevators also developed, thus adding to the functionality of buildings.

Skyscrapers, in which elevators are installed, have more floors and greater need for this kind of transport inside the building. This is why great requirements for security, number of passengers, energy efficiency, economical use of space and passenger comfort are set for the elevators nowadays. The fact that every year in the European Union 125000 new elevators are installed and that there are 4.3 million already installed elevators tells us about their significance in the society nowadays [1].

* Correspondence to: University in Banja Luka, Faculty of Mechanical Engineering, Vojvode Stepe Stepanovica 71, 78000 Banja Luka, Republic of Srpska, Bosnia and Herzegovina.
E-mail address: bojan.knezevic@mf.unibl.org (B.Z. Knezevic).

http://dx.doi.org/10.1016/j.jsv.2017.06.006
0022-460X/

The nominal speed of modern elevators is becoming faster in order to increase their availability in buildings with high frequency of traffic, implying the requirements for positioning with great precision. When these elevators start or stop, there is a huge jerk which has adverse time shape and it can cause discomfort of passengers and even exceed the value which human organism can endure [2].

The control of a jerk is not only important for the passengers and goods transported by elevators. Uncontrolled jerk value has adverse impact on power drive and the mechanical subsystem of an elevator, and especially on a drive sheave and a wire rope which are quickly prone to wear because of the slip that occurs. A number of ways of modeling speed reference are proposed in literature, such that during acceleration and deceleration a jerk has a desired shape and allowed amplitude. Usually square, trapezoidal and sine shapes of a jerk change are proposed [3,4]. A speed pattern which causes uncontrolled jerk, whose amplitude is far bigger than 2 m/s^3 [5], which is the jerk that human organism can endure, is shown in Fig. 1.

Not only that jerk control provides a comfortable ride and extends the life cycle of the EMS, but it also reduces the possibility for vibration to appear [6]. Namely, every EMS mechanical subsystem represents the system of two masses connected by a wire rope of finite stiffness. The mechanical subsystem of an elevator is characterized by resonant frequency, which is inside the bandwidth of the speed controller [7]. Any sudden change at the speed controller output acts like the excitation of the resonant circuit of a mechanical subsystem, which results in the occurrence of vibration and disables the function of the controller.

The speed controller should follow the speed reference, which is defined by a jerk, without an error. It can work only if the controller is in a linear mode and if it has gain which is big enough. The linear mode can be achieved by the right choice of the speed reference shape, that is, a jerk, while a big gain of a controller making rich harmonic spectrum, which also contains EMS resonant frequency, causes resonant vibrations.

Fig. 2 shows the time response of speed on step change of the drive torque for three values of the load in an elevator car. The figure shows that time responses of the speed have damped oscillation whose frequencies are equal to resonant frequency of the EMS mechanical subsystem. It is also clear that amplitude of oscillation depends on the load, and the fre-

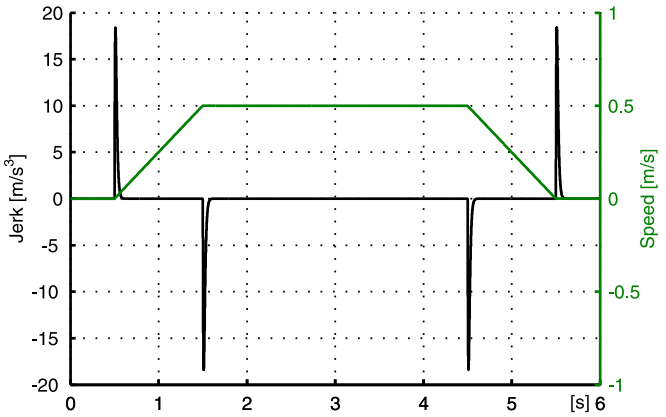

Fig. 1. The uncontrolled jerk due to non optimal trapezoidal shaped speed reference.

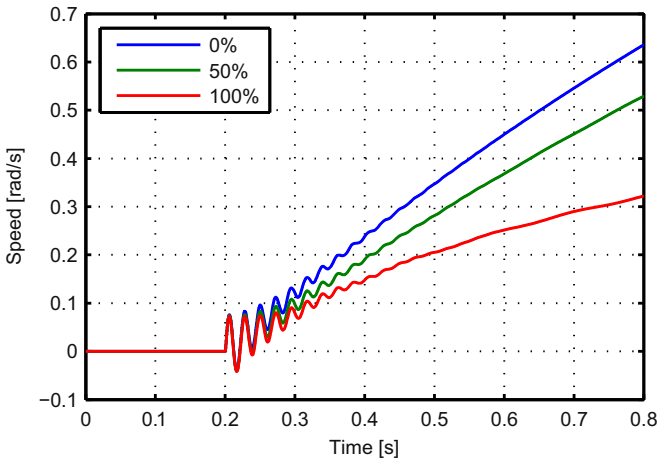

Fig. 2. The time response of the EMS on step torque reference for different loads in the elevator car.

quency does not.

Different approaches for suppression of vibration in general can be found in literature. If the sufficiently accurate mathematical model is known, then the resonant frequency can be determined analytically. Different models of wire ropes and mechanical subsystems are described in [8,9]. In one of those models authors described [10] a controller which dissipates vibration energy. The problem related to solutions which are based on the model is that they cannot be used if model parameters are not known. This is why authors in [11,12] recommended experimental ways, whereas authors in [13,14] recommend using a complex observer to determine the parameters of a mathematical model. The solution which is proposed in [13] requires a lot of computer resources. In [15] authors use control techniques which detect vibration indirectly on the basis of a mathematical model. The drawback of the recommended control techniques is that they require complex adjustment of numerous filters and phase shifters. There are solutions which suppress vibrations by installing additional devices on the elevator car [16].

One of the ways to suppress resonant vibration is to use band-stop filters [17] or other types, such as exponential filters [18]. The mathematical models of band-stop filters are analyzed in [19], and procedures for their adjustments applied on simple systems are described in [20]. Authors in [13] claim that using band-stop filters slows down speed controller dynamic response. If steel ropes are extremely long, resonant frequencies change with the position of the car [21,22]. Changing of the resonant frequencies can cause the problems with the filter based solutions.

This paper proposes integral solution which will solve the problem of an uncontrolled jerk and occurrence of resonant vibration without compromising dynamic features and the accuracy of the speed controller. Unlike previously presented solutions in the literature, a generalized model of generator speed references, which is defined by desired shape and amplitude jerk, is proposed in this paper. It is possible to choose any shape of the jerk from square to sine using a shape factor. Furthermore, it is possible to independently define the shape and amplitude of the jerk in the periods of acceleration and deceleration. The generalized model enables utilization of both shapes of the jerk, with and without intermediate zero periods, as well as the possibility of using the EMS with direct landing and limit switch type of positioning. The speed reference obtained using such a generator has the shape of smooth curve which a speed controller can follow easily and which can be adjusted so that the linear mode of the controller can be provided.

In the proposed solution the PID speed controller has optimal parameters for the fastest dynamic response and following reference without error. In order to remove the resonant component in spectrum torque reference, the speed controller is expanded by a band-stop filter. In this way a modified speed controller neutralizes vibrations, if the EMS resonant frequency is known and if it does not depend on the position of the car, without attenuation and without the phase shift of the reference torque. In order to determine resonant frequency, this paper proposes the procedure for determining the EMS resonant frequency which is based on frequency analysis and on the application of Goertzel algorithm and search algorithm. The proposed tuning procedure is an offline software procedure and it does not require additional devices.

The result of the proposed solution is a smooth start and halt of the elevator car without vibration with high precision of positioning and minimum duration time. All proposed algorithms are verified through computer simulation and experimentally on an EMS scale down prototype whose control subsystem is based on digital signal processor (DSP).

The development of the proposed solution starts with the derivation of an EMS mathematical model which is presented in Section 2. Detailed analysis of the occurrence of EMS resonant vibration with the mathematical model of the band-stop filter is given in Section 3. In Section 3 the proposed procedure for band-stop filter tuning is also described. Section 4 deals with the analysis of different jerk shapes and presents a mathematical model for proposed generalized generator of speed reference in the function of a jerk. The main contribution of this paper, the proposed anti-resonant and jerk free control scheme for the EMS, is described in Section 5. The experiments refer to the verification of the algorithms for vibration suppression and the model for jerk control. Technical prototype description of the EMS and results obtained in experimental tests are presented in Section 6. Conclusions based on the research described in this paper are listed in Section 7. Besides the abovementioned, every chapter also contains a review of recent research in the field of interest, and all cited literature is listed at the end of the paper.

2. The description and modeling of an elevator mechatronic system

The structure of a modern elevator system is presented in Fig. 3. Basically, the modern elevator is composed of a traffic control and an elevator mechatronic system. The traffic control of the modern elevator system is a computer based traffic manager of one or more elevators in the group. The traffic control is higher level control which dispatches elevator cars on passenger demand. The primitive traffic control was named “on-call” and it was for a single elevator. For modern elevators in the group the models of management schedules have been developed. They are based on computer programs and often on artificial intelligent networks [23].

The EMS is a lower level but a fundamental part of a modern elevator system. A block diagram of the EMS structure is presented in the dark gray block in Fig. 3. This paper deals with the EMS.

The EMS is composed of a mechanical subsystem, a power drive subsystem, a digital signal processor (DSP) control subsystem and software.

The mechanical subsystem of the EMS contains the following parts: an elevator car, a counterweight, a drive sheave, overhead sheaves and wire ropes (Fig. 4a). The mechanical subsystem is gearless, i.e. produced drive torque at the motor

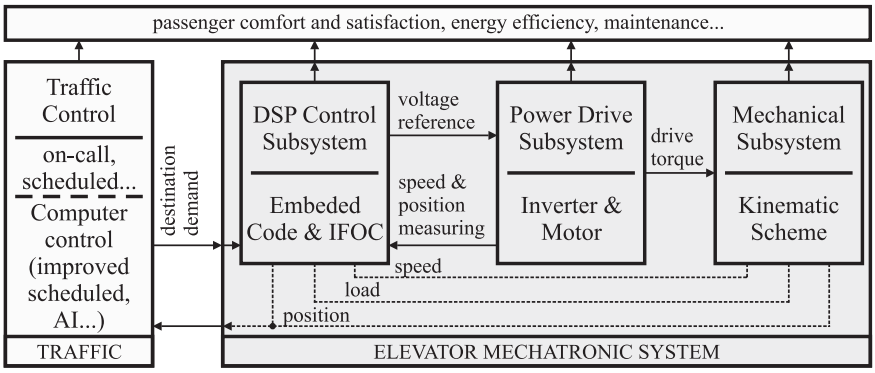

Fig. 3. The structure of a modern elevator system: the traffic control (light gray, left) and the elevator mechatronic system (dark gray, right). The performance of these two segments affects the quality of the overall elevator system (light gray, above).

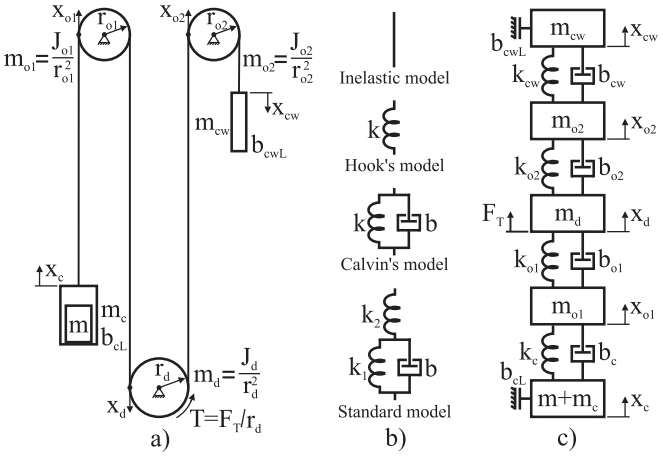

Fig. 4. a) The kinematic scheme of the EMS, b) Rheological models of the wire rope: Inelastic, Hook's, Calvin's and Standard model, c) The equivalent mechanical scheme of the kinematic scheme.

shaft is transferred directly to the driving sheave without the gearbox. The movement of the drive sheave is transmitted to the wire rope by means of friction force and V-grooves. Overhead sheaves serve for the appropriate placement of the elevator car and the counterweight (Fig. 4a).

The power drive subsystem performs two types of energy conversion. The electrical power from the power grid must be converted from the constant frequency and constant voltage to the variable frequency and variable voltage. The second is electro-mechanical conversion. In this paper the EMS is with a current regulated voltage source inverter (CRVSI) which feeds the squirrel cage induction three phase motor as an electro-mechanical converter. The algorithm for the power drive control is the indirect field oriented control (IFOC).

The DSP control subsystem is a microprocessor based control unit. The inputs of the control software are as follows: desired destination from the traffic control and measured speed, position, electrical current and load. The control software generates voltage reference for the power drive subsystem.

2.1. The mathematical model of the EMS mechanical subsystem

There are many different solutions for hanging the car and counterweight and, as a result, many kinematic schemes. This paper deals with the type of the EMS whose kinematic scheme is presented in Fig. 4a.

Dimensioning of the counterweight depends on the elevator capacity and the weight of an elevator car: $m_{cw}=m_c+m_{\max}/2$, where m_{cw} is the weight of the counterweight, m_c is the weight of an empty elevator car and $m_{\max}$ is elevator capacity.

There are various types of wire rope modeling. It depends on its purpose. A dynamical model of wire ropes is based on rheological model of material and could be modeled like inelastic body, Hook's ideal elastic body, Calvin's model and Standard model (Fig. 4b) [9]. The rope modeling as an inelastic body is useful for a simplified model of an elevator which is widely used for determination of basic relations between components of elevator mechanical subsystem, power drive dimensioning and synthesis of control structures. A vibration analysis has an important role in understanding and designing EMS. A simplified model of the elevators mechanical subsystem is not suitable for vibration analysis or another dynamical analysis. In most cases of dynamical analysis of EMS, the Calvin's model (Fig. 4b) of a wire rope is satisfactory [24].

The kinematic scheme from Fig. 4a could be represented as an equivalent mechanical scheme in Fig. 4c. The mechanical scheme from Fig. 4c consists of two lumped masses (an elevator car and a counterweight) and three inertia masses (overhead sheaves and a drive sheave. The wire rope which is between masses is modeled with the Calvin's model (Fig. 4b) composed of a spring of great stiffness and damping. The mass of the wire rope is neglected. For each mass from Fig. 4c, according to Newton's second low, is possible to write one linear differential equation of motion. Therefore, a mathematical model of the elevator equivalent mechanical scheme from Fig. 4c is a five degrees of freedom system and it is described by five linear differential equations ($m+m_c$: Eq. (1), m_{o1}: Eq. (2), m_d: Eq. (3), m_{o2}: Eq. (4) and m_{cw}: Eq. (5)) as follows:

$$(m + m_c)\ddot{x}_c + k_c(x_c - x_{o1}) + b_c(\dot{x}_c - \dot{x}_{o1}) + b_{c\,L}\dot{x}_c = 0, \tag{1}$$

$$m_{o1}\ddot{x}_{o1} + k_{o1}(x_{o1} - x_d) + b_{o1}(\dot{x}_{o1} - \dot{x}_d) + k_c(x_{o1} - x_c) + b_c(\dot{x}_{o1} - \dot{x}_c) = 0, \tag{2}$$

$$m_d\ddot{x}_d + k_{o1}(x_d - x_{o1}) + b_{o1}(\dot{x}_d - \dot{x}_{o1}) + k_{o2}(x_d - x_{o2}) + b_{o2}(\dot{x}_d - \dot{x}_{o2}) = F_T, \tag{3}$$

$$m_{o2}\ddot{x}_{o2} + k_{o2}(x_{o2} - x_d) + b_{o2}(\dot{x}_{o2} - \dot{x}_d) + k_{cw}(x_{o2} - x_{cw}) + b_{cw}(\dot{x}_{o2} - \dot{x}_{cw}) = 0, \tag{4}$$

$$m_{cw}\ddot{x}_{cw} + k_{cw}(x_{cw} - x_{o2}) + b_{cw}(\dot{x}_{cw} - \dot{x}_{o2}) + b_{cwL}\dot{x}_{cw} = 0, \tag{5}$$

where m are masses, x are displacements, k are equivalent stiffness, b are damping coefficients and F_T is a driving force. The subscript c indicates an elevator car, the subscript cw indicates a counterweight, the subscripts $o1$ and $o2$ indicate overhead sheaves and the subscript d indicates a drive sheave. The subscripts L along b denote the friction of linear movement between the steel guide rails and the elevator car and counterweight.

All terms in Eqs. (1)-(5) as well as in Fig. 4c are presented like linear motion terms. By substituting linear motion terms with rotational motion terms for the drive sheave, overhead sheaves and drive torque in Eqs. (1)-(5), the state space representation of the elevator kinematic scheme from Fig. 4a is as follows:

$$\dot{q}_m(t) = \mathbf{A_m}q_m(t) + \mathbf{B_m}u_m(t), \tag{6}$$

$$y_m(t) = \mathbf{C_m}q_m(t) + \mathbf{D_m}u_m(t), \tag{7}$$

where $q_m(t)$ is a state vector, $u_m(t)$ is input (drive torque) and $y_m(t)$ is output (speed). An $\mathbf{A_m}$ (system matrix), $\mathbf{B_m}$ (input vector), $\mathbf{C_m}$ (output vector) and $\mathbf{D_m}$ (feedthrough) are given below, respectively:

$$\mathbf{A_m} = \begin{bmatrix}
0 & 1 & 0 & 0 & 0 & 0 & 0 & 0 & 0 & 0 \\
\frac{-k_c}{m+m_c} & \frac{-(b_c+b_{cL})}{m+m_c} & 0 & 0 & 0 & 0 & \frac{k_c r_{o1}}{m+m_c} & \frac{b_c r_{o1}}{m+m_c} & 0 & 0 \\
0 & 0 & 0 & 1 & 0 & 0 & 0 & 0 & 0 & 0 \\
0 & 0 & \frac{-k_{cw}}{m_{cw}} & \frac{-(b_{cw}+b_{cwL})}{m_{cw}} & 0 & 0 & 0 & 0 & \frac{k_{cw}r_{o2}}{m_{cw}} & \frac{b_{cw}r_{o2}}{m_{cw}} \\
0 & 0 & 0 & 0 & 0 & 1 & 0 & 0 & 0 & 0 \\
0 & 0 & 0 & 0 & \frac{-r_d^2(k_{o1}+k_{o2})}{J_d} & \frac{-r_d^2(b_{o1}+b_{o2})}{J_d} & \frac{k_{o1}r_d r_{o1}}{J_d} & \frac{b_{o1}r_d r_{o1}}{J_d} & \frac{k_{o2}r_d r_{o2}}{J_d} & \frac{b_{o2}r_d r_{o2}}{J_d} \\
0 & 0 & 0 & 0 & 0 & 0 & 0 & 1 & 0 & 0 \\
\frac{k_c r_{o1}}{J_{o1}} & \frac{b_c r_{o1}}{J_{o1}} & 0 & 0 & \frac{k_{o1}r_d r_{o1}}{J_{o1}} & \frac{b_{o1}r_d r_{o1}}{J_{o1}} & \frac{-r_{o1}^2(k_c+k_{o1})}{J_{o1}} & \frac{-r_{o1}^2(b_c+b_{o1})}{J_{o1}} & 0 & 0 \\
0 & 0 & 0 & 0 & 0 & 0 & 0 & 0 & 0 & 1 \\
0 & 0 & \frac{k_{cw}r_{o2}}{J_{o2}} & \frac{b_{cw}r_{o2}}{J_{o2}} & \frac{k_{o2}r_d r_{o2}}{J_{o2}} & \frac{b_{o2}r_d r_{o2}}{J_{o2}} & 0 & 0 & \frac{-r_{o2}^2(k_{cw}+k_{o2})}{J_{o2}} & \frac{-r_{o2}^2(b_{cw}+b_{o2})}{J_{o2}}
\end{bmatrix}$$

$$\mathbf{B_m} = \begin{bmatrix} 0 & 0 & 0 & 0 & 0 & \frac{1}{J_d} & 0 & 0 & 0 & 0 \end{bmatrix}^{\mathrm{T}},\ \mathbf{C_m} = \begin{bmatrix} 0 & 0 & 0 & 0 & 0 & 1 & 0 & 0 & 0 & 0 \end{bmatrix} \text{ and } \mathbf{D_m} = 0.$$

The load torque on the motor shaft, T_{load} as well as the moment of inertia of the whole mechanical subsystem, J_{load} depend on the mechanical subsystem parameters and mass in the elevator car (and acceleration due to gravity, g_n):

$$T_{\mathrm{load}} = r_d{\cdot}(m_c + m - m_{cw}){\cdot}g_n, \tag{8}$$

$$J_{\mathrm{load}} = J_d + J_{o1} + J_{o2} + r_d^2{\cdot}(m_c + m + m_{cw}) \tag{9}$$

2.2. The mathematical model of the EMS power drive subsystem

As briefly described before, the elevator power drive subsystem is composed of a power converter and a motor. The power converter has negligible influence on EMS dynamics, so in this paper the voltage source inverter is modeled as an ideal voltage amplifier. Therefore, the mathematical model of the power converter is gain V_{DC}.

A widely used motor in the EMS is an induction three phase motor with a squirrel cage rotor. This type of the motor is very robust, durable, low-cost and almost maintenance free. The original dynamic model of the induction motor is a three phase model named *abc* model composed of differential and algebraic equations. Complexity simplification of the original dynamic model is realized by using Clarke's transformation which transforms original phase quantities (a, b and c) into equivalent two phase quantities (α and β). Further simplification can be made using Park transformation which maps stationary $\alpha\beta$ to rotating dq reference frame.

The dynamic model of the induction motor in dq reference frame for both stator and rotor is given as follows:

$$\mathbf{v_s} = R_s \cdot \mathbf{i_s} + \dot{\mathbf{\Psi}}_\mathbf{s} + \mathrm{j}\omega_{dq}\mathbf{\Psi_s}, \tag{10}$$

$$\mathbf{v_r} = R_r \cdot \mathbf{i_r} + \dot{\mathbf{\Psi}}_\mathbf{r} + \mathrm{j}(\omega_{dq} - \omega_r)\mathbf{\Psi_r} = \mathbf{0}, \tag{11}$$

$$\mathbf{\Psi_s} = L_s \cdot \mathbf{i_s} + L_m \cdot \mathbf{i_r}, \tag{12}$$

$$\mathbf{\Psi_r} = L_m \cdot \mathbf{i_s} + L_r \cdot \mathbf{i_r}, \tag{13}$$

where j is a complex operator and $\mathbf{v}$, $\mathbf{i}$ and $\mathbf{\Psi}$ are vectors of voltages, currents and fluxes, respectively:

$$\mathbf{v_s} = \begin{bmatrix} v_{sd} & v_{sq} \end{bmatrix}^T, \mathbf{i_s} = \begin{bmatrix} i_{sd} & i_{sq} \end{bmatrix}^T, \mathbf{\Psi_s} = \begin{bmatrix} \Psi_{sd} & \Psi_{sq} \end{bmatrix}^T, \mathbf{v_r} = \begin{bmatrix} v_{rd} & v_{rq} \end{bmatrix}^T, \mathbf{i_r} = \begin{bmatrix} i_{rd} & i_{rq} \end{bmatrix}^T, \mathbf{\Psi_r} = \begin{bmatrix} \Psi_{rd} & \Psi_{rq} \end{bmatrix}^T.$$

Motor parameters are the stator windings resistance R_s, the rotor windings resistance R_r, the stator self inductance L_s, the rotor self inductance L_r and the mutual inductance L_m. The subscripts s denote stator variables and r rotor variables. Speeds are denoted with ω_{dq} for the synchronous speed and ω_r for the mechanical speed of the rotor. The subscript d is for the direct component of quantities (on d axis) and the subscript q is for the quadrature component of quantities (on q axis).

The system Eqs. (10)-(13) can be expressed in the form of a state space model Eq. (14) and Eq. (15):

$$\dot{q}_e(t) = \mathbf{A_e} q_e(t) + \mathbf{B_e} u_e(t), \tag{14}$$

$$y_e(t) = \mathbf{C_e} q_e(t) + \mathbf{D_e} u_e(t) \tag{15}$$

Commonly used state variables are rotor flux and stator current vectors. The matrices of the system Eq. (14) and Eq. (15) are defined as:

$$q_e(t) = [i_{sd} \quad i_{sq} \quad \Psi_{rd} \quad \Psi_{rq}]^T,$$

$$u_e(t) = \begin{bmatrix} v_{sd} & v_{sq} \end{bmatrix}^T, y_e(t) = \begin{bmatrix} i_{sd} & i_{sq} \end{bmatrix}^T,$$

$$\mathbf{A_e} = \begin{bmatrix} -\frac{1}{\tau_\sigma} & \omega_{dq} & \frac{L_m}{L_\sigma L_r \tau_r} & \frac{L_m \omega_r}{L_\sigma L_r} \\ -\omega_{dq} & -\frac{1}{\tau_\sigma} & -\frac{L_m \omega_r}{L_\sigma L_r} & \frac{L_m}{L_\sigma L_r \tau_r} \\ \frac{L_m}{\tau_r} & 0 & -\frac{1}{\tau_r} & \omega_{dq} - \omega_r \\ 0 & \frac{L_m}{\tau_r} & \omega_{dq} - \omega_r & \frac{1}{\tau_r} \end{bmatrix}, \mathbf{B_e} = \begin{bmatrix} \frac{1}{L_\sigma} & 0 & 0 & 0 \\ 0 & \frac{1}{L_\sigma} & 0 & 0 \end{bmatrix}^T, \mathbf{C_e} = \begin{bmatrix} 1 & 0 & 0 & 0 \\ 0 & 1 & 0 & 0 \end{bmatrix}, \text{ and } \mathbf{D_e} = 0,$$

where are: $\tau_r = \frac{L_r}{R_r}$, $L_\sigma = L_s\left(1 - \frac{L_m^2}{L_s L_r}\right)$, $R_\sigma = R_s + R_r \frac{L_m^2}{L_r^2}$, $\tau_\sigma = \frac{L_\sigma}{R_\sigma}$.

The mechanical equation of the EMS power drive subsystem is:

$$\frac{\mathrm{d}\omega_r}{\mathrm{d}t} = \frac{T_{el} - T_{\mathrm{load}}}{J_m}, \tag{16}$$

where J_m is the moment of inertia of the rotor. If P denotes the number of the pole pairs of the motor, T_{el} is the torque generated by the induction motor:

$$T_{el} = \frac{3}{2} P \frac{L_m}{L_r} (\Psi_{rd} i_{sq} - \Psi_{rq} i_{sd}) \tag{17}$$

2.3. The mathematical model of the IFOC control scheme

The stator voltage Eq. (10) can be reduced by using the CRVSI. The CRVSI regulates the stator voltage vector until the commanded stator current vector is injected into the motor. If the rotor flux vector angle is known, the stator current vector

can be regulated in a way to insure that only the q-axis current component produces torque and, at the same time, the d-axis current controls the rotor flux level. As a consequence, the induction motor model Eqs. (10)-(17) is reduced to Eqs. (18)-(19), which are the main result of the IFOC:

$$T_{el} = \frac{3}{2}P\frac{L_m}{L_r}\Psi_{rd}i_{sq} = k_{Tel}i_{sq}, \tag{18}$$

$$\Psi_{rd} = \frac{L_m}{s\tau_r + 1}i_{sd} \tag{19}$$

The block structure of an IFOC algorithm is shown in Fig. 5. It contains two main parts. The first part is the CRVSI which insures the injection of commanded stator currents. The CRVSI is realized in the rotating dq frame with two independent PI current controllers. Both controllers react to the difference between the measured (i_{sd} and i_{sq}) and commanded (i^*_{sd} and i^*_{sq}) currents and regulate the corresponding dq voltage components, v^*_{sd} and v^*_{sq}. These voltages are transformed over Inverse Park's transformation to stationary reference frame (v^*_{α} and v^*_{β}) and fed to the Space Vector Modulator which generates the corresponding PWM signals. The second part of the IFOC structure is a flux estimator in which rotor flux vector amplitude and angle are estimated. The IFOC flux estimator is based on the induction motor model, especially on the Eq. (11), and calculates the slip frequency which insures zero rotor flux in the q-axis. The flux estimator calculates the Eq. (20) in real time:

$$\theta_{dq} = \theta_r + \frac{1}{s}\left(\frac{L_m}{\tau_r\hat{\Psi}_{rd}}i_{sq}\right),\ \hat{\Psi}_{rd} = \frac{L_m}{s\tau_r + 1}i_{sd}, \tag{20}$$

where s is a complex variable and \widehat denotes estimated value.

The linear torque control, ensured by the IFOC, is a base requirement for the linear speed and the position control of the EMS, which will be explored in the following sections.

2.4. The speed and position control model of the EMS

The EMS is basically a position control system. For the position control the EMS uses the position reference pattern whose final value is the final position of the elevator car L (dot lines in Fig. 6). But in practice the EMS implementation with the position feedback control is very rear. A much more common case in practice is the speed controlled EMS in which the final position of the elevator car is determined by limit switches at each floor. That specific position control is based on the real time tracking of the speed trajectory. The input parameter for speed trajectory generation is the final position of the elevator car L. The generated speed trajectory ensures that the desired position at the end of a ride is achieved. A possible speed tracking error causes the position error which is eliminated via the limit switch. The switch reacts to the defined final position and stops the elevator car (solid lines in Fig. 6).

At the speed controlled EMS the final value of the speed reference trajectory is not zero. The final value of the speed reference is a small constant value which is the landing speed for coming to the final position. The landing speed is defined by the landing factor $\upsilon\epsilon[0,1]$ such that $\upsilon \cdot V \cdot 100$ is the percentage of the rated elevator speed V (Fig. 6).

The speed trajectory, the position of the elevator car and the limit switch action during deceleration are shown in Fig. 6.

The main task of the speed controller is to track the speed reference trajectory. If the speed trajectory has a smooth shape with a limited slope to insure controller operation between permissible torque limits than speed controller operates in a linear mode. Therefore, for a strictly linear mode of operation the linear controller such as a PI controller is suitable.

Generated speed reference must be tracked without errors. In order to meet this requirement there must be both proportional and integral action of the PI controller in the direct path. An aperiodic character of the speed response without

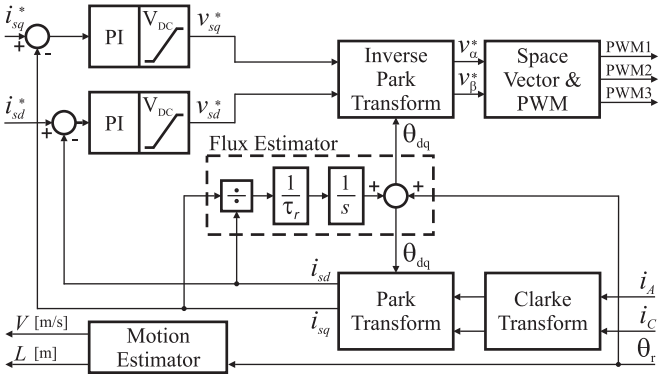

Fig. 5. The decoupled control of flux and torque applying the IFOC control algorithm which is implemented in the DSP based control subsystem.

overshoot is required. Also, the response should be the fastest as practicable. The structure of the speed controller which satisfies all listed specifications is shown in Fig. 7. It is a PI controller in incremental form for which parameter setting is derived in [25].

The control signal at the output of the PI controller is limited with the positive and negative maximum drive torque, T_{max}. In the linear mode of operation a limiter should be inactivated. The feedback signal is the speed of linear movement of the elevator car, V [m/s].

3. The vibration suppression suitable for an elevator mechatronic system

An ordinary speed or position control is not enough for proper operation of the EMS. Vibration, which is mainly caused by finite stiffness of the wire rope, is a disturbing factor that makes it difficult to control the speed, undermines the comfort of the passengers and causes damage to the elements of the mechanical subsystem. This section analyzes characteristics of vibration in the EMS, describes a solution for vibration suppression and defines a procedure for the implementation of proposed solution.

3.1. The analysis of the EMS vibration phenomenon

It can be seen from Fig. 2 given in Introduction that speed responses have damped oscillations caused by the finite stiffness of the wire rope. For the frequency analysis Bode diagrams are more suitable. Fig. 8 shows the Bode diagrams of the EMS. As can be seen, the EMS has one resonant frequency which depends only on the elevator construction and not on the elevator load. The elevator load affects the rest of frequency characteristic but does not cause additional resonant frequencies. Frequencies above 10^3 rad/s are not necessary to be analyzed because they are significantly out of the speed controller bandwidth.

Owing to the optimized but large gains, the torque reference at the output of the speed controller T_{el}^{*} (Fig. 7) has a rich spectrum including the resonant frequency of the EMS [25]. The torque reference excites the resonant vibrations and corrupts the speed control as well as the position accuracy. Filtering of the resonant frequency component from the torque reference spectrum and therefore expansion of the applicable speed controller gains will solve the vibration and speed control problem.

An appropriate procedure for the indicated task is band-stop filtering. Filtering has the task to change the frequency characteristics of the EMS in the resonant frequency region. The selected band-stop filter and the procedure proposed for its tuning are discussed in the following subsections.

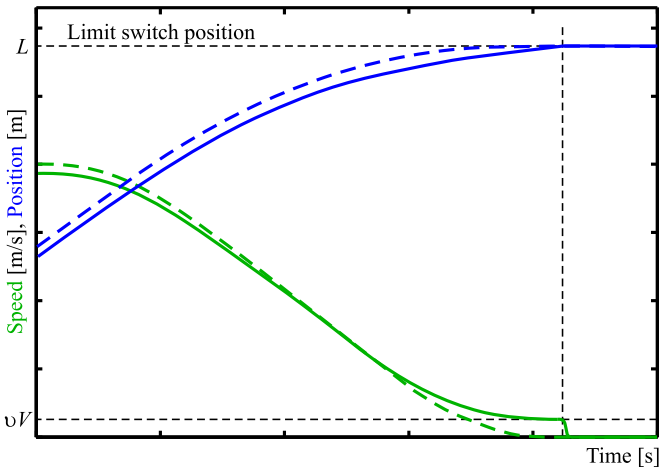

Fig. 6. The speed trajectory and the limit switch reaction during the deceleration and stopping.

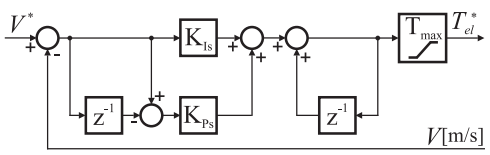

Fig. 7. The structure of the PI speed controller in the incremental form.

3.2. The design of a vibration suppression filter

The resonant frequency of the EMS is caused by a pair of conjugate complex poles. The band-stop filter should have the same pair of conjugate complex zeros to annul resonant poles of the EMS. Also, the band-stop filter should have one pair of conjugate complex poles which will replace canceled resonant poles at the same frequency, but well damped. The transfer function of the band-stop filter which has a required configuration with two poles and two zeros at resonant (center) frequency ω_0 could be written as:

$$G_{BS}(s) = \frac{s^2 + 2\varsigma_Z\omega_0 s + \omega_0^2}{s^2 + 2\varsigma_P\omega_0 s + \omega_0^2}, \tag{21}$$

where ς_Z and ς_P are zero and pole damping factors, respectively. The band-stop filter is defined with three parameters: ω_0, ς_Z and ς_P. Fig. 9 shows magnitude characteristic of a well-tuned band-stop filter ($|G_{BS}|$). The same figure shows the magnitude characteristics of the EMS with a well-tuned band-stop filter ($|G_{EF}|$) and without filtering ($|G_E|$). The input of the filter is the torque reference T_{el}^* and output is the quadrature current reference, i_q^* (Fig. 13).

The proper adjustment of the filter poles and zeros produces attenuation on the resonant frequency and in the neighborhood of the resonant frequency (Fig. 9). The filter does not cause any additional attenuation on other frequencies.

The implementation of a band-stop filter on the DSP requires discrete and difference representation of Eq. (21). The infinite impulse response (IIR) design of the band-stop filter is used for DSP algorithm implementation and its discrete equation is [8]:

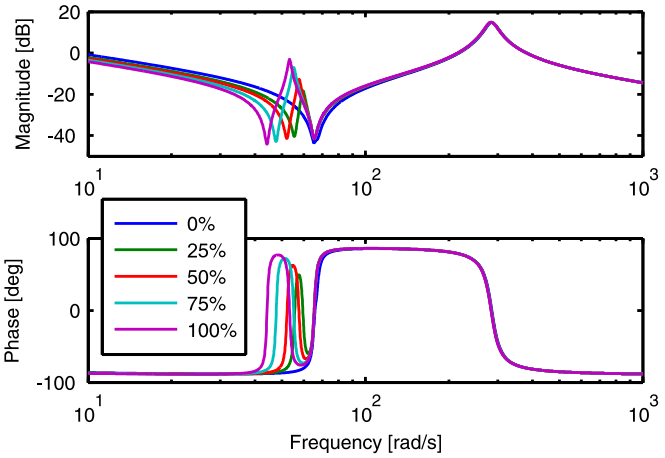

Fig. 8. The frequency response of the EMS from the drive torque to the speed for different loads.

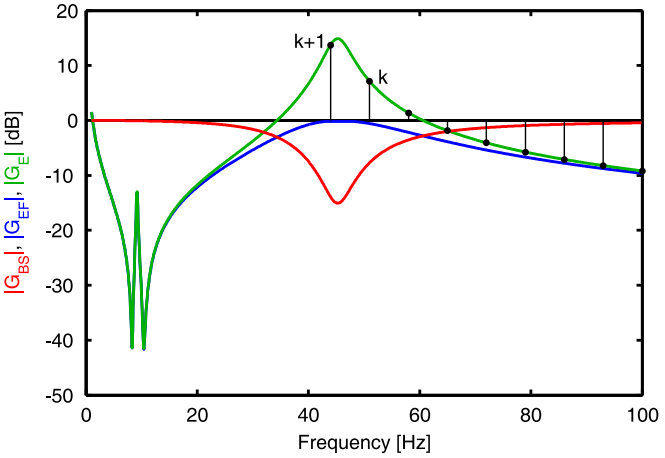

Fig. 9. The magnitude response against frequency of a well-tuned band-stop filter and the magnitude response against frequency of the EMS with and without a filter.

$$G_{BS}(z) = \frac{\Lambda_1 z^2 - \Lambda_2 z + \Lambda_3}{z^2 - \Lambda_4 z + \Lambda_5}, \tag{22}$$

where z is the discrete operator and constants are as follows:

$$\begin{aligned}
\Lambda_1 &= \exp[-(\varsigma_P - \varsigma_Z)\omega_0\tau_{\text{filt}}],\\
\Lambda_2 &= 2\cos(\omega_0\tau_{\text{filt}}\sqrt{1-\varsigma_Z^2})\exp(-\varsigma_P\omega_0\tau_{\text{filt}}),\\
\Lambda_3 &= \exp[-(\varsigma_P + \varsigma_Z)\omega_0\tau_{\text{filt}}],\\
\Lambda_4 &= 2\cos(\omega_0\tau_{\text{filt}}\sqrt{1-\varsigma_P^2})\exp(-\varsigma_P\omega_0\tau_{\text{filt}}),\\
\Lambda_5 &= \exp(-2\varsigma_P\omega_0\tau_{\text{filt}}).
\end{aligned} \tag{23}$$

The time period τ_{filt} is a sampling period of the band-stop filter. Difference equation of Eq. (22) can be written and programed in the DSP code as:

$$T^*_{elO}(n) = \Lambda_1 T^*_{el}(n) - \Lambda_2 T^*_{el}(n-1) + \Lambda_3 T^*_{el}(n-2) + \Lambda_4 T^*_{elO}(n-1) - \Lambda_5 T^*_{elO}(n-2), \tag{24}$$

where T^*_{elO} is the output of the filter and n is the number of the sample. The filter Eq. (22) attenuate torque signal so the output of the filter must be boosted:

$$T^*_{elF}(n) = \Lambda_g \cdot T^*_{elO}(n),\ \Lambda_g = \frac{1 - \Lambda_4 + \Lambda_5}{\Lambda_1 - \Lambda_2 + \Lambda_3} \tag{25}$$

If the filter needs to attenuate more resonant frequencies ($N_{\omega o}$), than Eq. (24) and Eq. (25) will be repeated $N_{\omega o}$ times. Output from the one iteration is the input for the next iteration and so on. In each iteration Eq. (23) are different and tuned separately for different resonant frequency.

3.3. The proposed procedure for vibration suppression filter tuning

If all parameters in the model of the elevator mechanical subsystem are known, the band-stop filter parameters could be obtained from the system Eqs. (6)-(7). In practice it is a very rear case when all parameters in the model Eqs. (6)-(7) are known. The resonant frequency mostly depends on wire rope characteristics which are difficult to measure or calculate. Therefore, it is desirable to develop a method to adjust the filter that is not based on the model. The first task of filter parameters determination is to determine the all center frequencies which are equal to the resonant frequencies of the EMS. This task could be mapped into finding the maximums of the magnitude response function. Search algorithms are suitable for finding the maximum through the set of measurements.

One of the fastest search algorithms for determining maximum of the strictly unimodal function is the Kiefer's golden section search algorithm (GSS) [26]. The magnitude spectrum of the EMS is not unimodal on the entire frequency range for all loads (Fig. 8 and Fig. 10). So, before the implementation of the GSS algorithm it is necessary to find the frequency range in the neighborhood of the each resonant frequency which has only one maximum.

A pre-search (PS) procedure for determination of the all unimodal frequency ranges can be a series of successive excitations with the sine torque reference (T^*_{el}). Frequencies of the excitation torque are decreasing series of equidistant values which start from the highest frequency in the system (Fig. 9) and stops at the frequency close to zero. The highest vibration

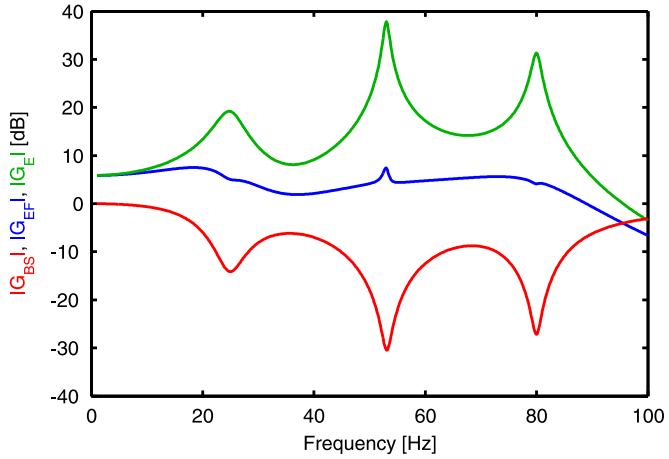

Fig. 10. The magnitude response against frequency of a well-tuned band-stop filter and the magnitude response against frequency of the EMS with and without a filter for case of three resonant frequencies.

frequency which influences EMS operation is determined by the speed controller bandwidth: $1/\tau_{speed}$. The criterion for unimodal frequency range in the neighborhood of the each resonant frequency is transition from negative to positive sign of derivation computed at each measured frequency by: $diff(k) = (G_E(\omega_{k+1}) - G_E(\omega_k)) / (\omega_{k+1} - \omega_k)$ where $|G_E(\omega)|$ is a magnitude of the measured speed and k is the number of excitation. At the end the PS procedure gives starting frequency ranges for the GSS algorithm in form $[\omega_{k+1}, \omega_k]$ for each resonant frequency. In Fig. 9 is shown example for one resonant frequency.

The GSS algorithm at the given frequency range calculates two new frequencies according to Eq. (26) and Eq. (27):

$$\omega_\alpha = \omega_k - \varphi(\omega_k - \omega_{k+1}), \tag{26}$$

$$\omega_\beta = \omega_{k+1} + \varphi(\omega_k - \omega_{k+1}), \tag{27}$$

where $\varphi = (1 + \sqrt{5})/2$ is a golden ratio [26]. The excitation of the EMS at frequencies $_{\omega\alpha}$ and $_{\omega\beta}$ gives new narrow range. If $|G_E(_{\omega\alpha})| > |G_E(\omega_\beta)|$ then the resonant frequency is in the new range: $[\omega_{k+1}, \omega_\beta]$. Otherwise, if $|G_E(\omega_\alpha)| < |G_E(_{\omega\beta})|$ the new range with the resonant frequency is: $[\omega_\alpha, \omega_k]$. The next iteration uses Eq. (26) and Eq. (27) for determination of the new frequency range and so on. If the difference between two successive frequencies is less then predefined error tolerance ε, the GSS algorithm is stopped and the procedure is finished. This procedure shall be repeated to determine all resonant frequencies.

Fig. 10 shows magnitude characteristic of a well-tuned band-stop filter ($|G_{BS}|$) for the EMS system with three resonant frequencies obtained through computer simulation. The same figure shows the magnitude characteristics of the EMS with a well-tuned band-stop filter ($|G_{EF}|$) and without filtering ($|G_E|$).

Both the GSS and the PS algorithms require the measurement of the speed magnitude $|G_E(\omega)|$. That is the maximal amplitude of the sine function which has the same frequency as the torque reference T^*_{el}. For maximal amplitude of the speed at the desired frequency this paper proposes the Goertzel algorithm. The Goertzel algorithm is the recursive scheme for computation of the discrete Fourier transformation [27]:

$$v_\kappa(n) = \omega_m(n) + 2\cos\left(\frac{2\pi\kappa}{N}\right)v_\kappa(n-1) - v_\kappa(n-2) \tag{28}$$

The original Goertzel algorithm has computations of the complex numbers. The modified Goertzel algorithm which has only real multiplications is more suitable for the DSP realization and computes the square magnitude Eq. (29) after N iterations of Eq. (28):

$$|G_E(\kappa)|^2 = v_\kappa^2(N) + v_\kappa^2(N-1) - 2\cos\left(\frac{2\pi\kappa}{N}\right)v_\kappa(N)v_\kappa(N-1) \tag{29}$$

In Eq. (28) and Eq. (29) N is the Goertzel block size, $0 \le n \le N$, $\nu_\kappa(n)$ is a state variable and ω_m is mechanical angular speed. The N is the frequency resolution of the algorithm and κ is an integer which selects a certain frequency. If f denotes frequency generated from the PS or the GSS algorithm and $f_{Goertzel}$ denotes the sampling frequency of the modified Goertzel algorithm then the Goertzel block size N adjusts its value to obtain a desired frequency according to:

$$N = \kappa \cdot f_{Goertzel}/f \tag{30}$$

The Goertzel algorithm does not calculate the actual amplitude of the signal, but rather the energy of the signal. Therefore, the final result depends on the signal length and must be rescaled to get the real amplitude value as follows:

$$|G_E(f)|^2_{abs} = |G_E(\kappa)|^2\left(\frac{2}{f_{Goertzel}\cdot\tau_d}\right)^2, \tag{31}$$

where τ_d [s] is duration of the measured signal.

The PS and the GSS algorithms determine resonant frequency of the EMS and the resonant magnitude. For the band-stop filter tuning it is necessary to determine damping factors ς_Z and ς_P, too.

At the center frequency, the frequency characteristic of the filter is real, phase is zero and ratio ς_Z/ς_P is equal to $|G_{BS}(\omega_0)|$. Taking into account this ratio as well as the relationship between magnitude characteristics of the EMS and the filter for the frequencies around resonant frequency: $|G_{BS}(\omega)| = 1/|G_E(\omega)|$, damping factors can be obtained as:

$$\varsigma_Z = \left|\frac{f_0^2 - f_a^2}{2f_0 f_a}\sqrt{\frac{|G_{Ea}|^2 - T^{*2}_{el}}{|G_{E0}|^2 - |G_{Ea}|^2}}\right|, \tag{32}$$

$$\varsigma_P = \varsigma_Z\cdot|G_{E0}|/T^*_{el}. \tag{33}$$

For the complete tuning of the filter Eq. (24) (i.e. calculation of parameters Eq. (23), Eq. (32) and Eq. (33)) are required: resonant frequency f_0 [Hz], magnitude of the angular speed at resonant frequency $|G_{E0}|$ [rad/s], any additional frequency f_a [Hz] around resonant frequency and its amplitude $|G_{Ea}|$ [rad/s].

4. The speed trajectory in the function of the jerk

Keeping the controller in a linear operation mode during the whole ride is crucial for the speed control of the EMS. This can be achieved by using the smooth shaped reference rather than the ramp or the step reference of the speed [25]. An indication of the speed reference smoothness is the shape and amplitude of jerk. In this Section the analysis of different jerk patterns is presented and a general model of speed reference defined by the jerk is proposed.

4.1. The analysis of jerk trajectory shapes

There are various shapes of jerk in literature. Fig. 11 shows most common shapes of the jerk: square, trapezoidal and sine as well as a quasi-trapezoidal shape which is a combination of the sine and cosine functions and constant values [28]. The advantage of the quasi-trapezoidal shape is a smooth transition from the constant slope period to the constant value period. Intermediate zero periods are an additional difference between various shapes of jerk patterns. Some jerk patterns have [29] and some do not have [30] an intermediate zero period. The intermediate zero period affects power drive utilization and ride duration.

The practice of the EMS design requires testing including various types of jerk patterns. A mathematical function of the speed or the position trajectory based on the controlled jerk are often very complex and require too much time for derivation and practical implementation. One single generalized mathematical model of the speed trajectory derived for the various types of jerk patterns is desirable. A general model of the speed trajectory defined by the jerk is derived and described in the next subsection. The proposed general model is a flexible solution for testing and designing process of the power drive in interaction with the mechanical subsystem as well as the synthesis of control loops.

4.2. The general model of the speed reference defined by the jerk

The starting point for derivation of the general model of the jerk pattern is a quasi-trapezoidal shape with intermediate zero periods. Sine and square shapes could be special cases of the quasi-trapezoidal shape. Definition of the quasi-trapezoidal jerk pattern is given using sine and cosine functions and constant values separated in strictly defined time periods (Fig. 12):

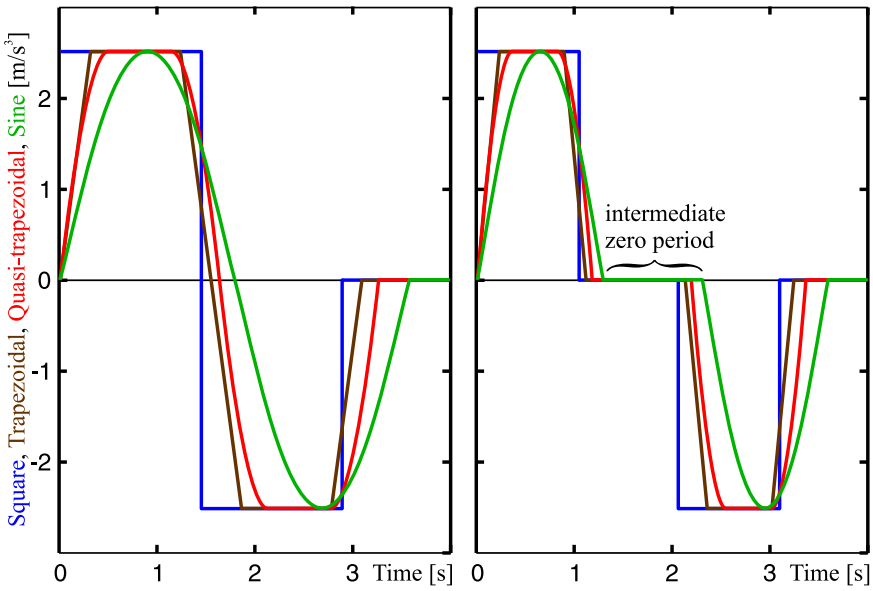

Fig. 11. Square, trapezoidal, quasi-trapezoidal and sine jerk patterns without and with intermediate zero periods.

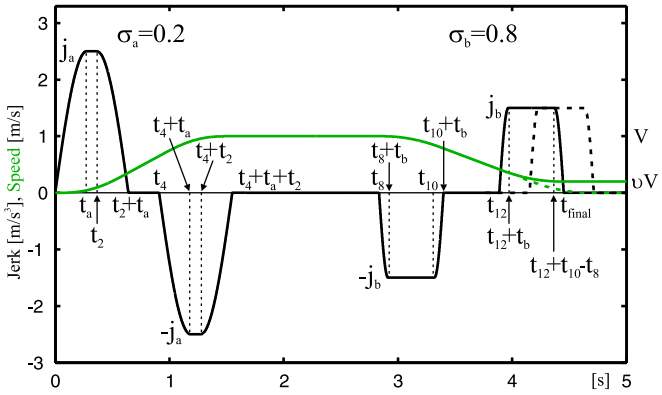

Fig. 12. The proposed speed trajectory based on the generalized jerk pattern with an intermediate zero periods.

$$
\begin{aligned}
&j_1(t) = j_a \sin\left(\frac{\pi}{2t_a}t\right), && t \in [0,\ t_a)\\
&j_2(t) = j_a, && t \in [t_a,\ t_2)\\
&j_3(t) = j_a \cos\left(\frac{\pi}{2t_a}(t - t_2)\right), && t \in [t_2,\ t_2 + t_a)\\
&j_4(t) = 0, && t \in [t_2 + t_a,\ t_4)\\
&j_5(t) = -j_a \sin\left(\frac{\pi}{2t_a}(t - t_4)\right), && t \in [t_4,\ t_4 + t_a)\\
&j_6(t) = -j_a, && t \in [t_4 + t_a,\ t_4 + t_2)\\
&j_7(t) = -j_a \cos\left(\frac{\pi}{2t_a}(t - t_2 - t_4)\right), && t \in [t_4 + t_2,\ t_4 + t_2 + t_a)\\
&j_8(t) = 0, && t \in [t_4 + t_2 + t_a,\ t_8)\\
&j_9(t) = -j_b \sin\left(\frac{\pi}{2t_b}(t - t_8)\right), && t \in [t_8,\ t_8 + t_b)\\
&j_{10}(t) = -j_b, && t \in [t_8 + t_b,\ t_{10})\\
&j_{11}(t) = -j_b \cos\left(\frac{\pi}{2t_b}(t - t_{10})\right), && t \in [t_{10},\ t_{10} + t_b)\\
&j_{12}(t) = 0, && t \in [t_{10} + t_b,\ t_{12})\\
&j_{13}(t) = j_b \sin\left(\frac{\pi}{2t_b}(t - t_{12})\right), && t \in [t_{12},\ t_{12} + t_b)\\
&j_{14}(t) = j_b, && t \in [t_{12} + t_b,\ t_{12} + t_{10} - t_8)\\
&j_{15}(t) = j_b \cos\left(\frac{\pi}{2t_b}(t - t_{12} - t_{10} + t_8)\right), && t \in [t_{12} + t_{10} - t_8,\ t_{final})\\
&j_{16}(t) = 0, && t \geq t_{final}.
\end{aligned}
\tag{34}
$$

In Eq. (34) $j_1(t)$- $j_{16}(t)$ are jerk functions which are user defined: j_a-the maximum amplitude of the jerk during acceleration and j_b-the maximum amplitude of the jerk during deceleration as well as times: t_a, t_2, t_4, t_8, t_b, t_{10}, t_{12} and t_{final} which are determined with certain mathematical relations as follows (Fig. 12).

Time t_a and time t_b are obtained from the definitions of the jerk and they are:

$$t_a = \sigma_a \frac{\pi A_a}{4j_a}, \tag{35}$$

$$t_b = \sigma_b \frac{\pi A_b}{4j_b}, \tag{36}$$

where A_a and A_b are the desired maximum amplitude of acceleration and deceleration, respectively. Coefficient $\sigma_a \epsilon [0,1]$ is the shape factor of the jerk pattern in an acceleration period and $\sigma_b \epsilon [0,1]$ is the shape factor of the jerk pattern in a

deceleration period. The shape factor defines the shape of the jerk pattern as follows: for $\sigma = 0$ the square shape, for $\sigma = 1$ the sine shape and for $\sigma \in (0,1)$ the quasi-trapezoidal shape with adjustable slope and curvature.

After derivation of the acceleration function based on the jerk pattern Eq. (34) using the relation between acceleration and jerk: $a(t) = \int j(t)dt$, time t_2 and time t_{10} are obtained as follows:

$$t_2 = \frac{A_a}{j_a} - \frac{4}{\pi}t_a + t_a, \tag{37}$$

$$t_{10} = \frac{A_b}{j_b} - \frac{4}{\pi}t_b + t_b + t_8 \tag{38}$$

The relation between speed and acceleration $v(t) = \int a(t)dt$ gives a speed function. Rated speed of the elevator car (V) is one of the main elevator parameters. Some speed patterns in literature do not have the period of constant speed [31], which is debatable, because elevators are equipped with protective devices like a speed governor that monitors the speed of the elevator car. Times t_4 and t_{12} can be calculated as a function of rated elevator speed (V) and the maximum amplitude for acceleration and deceleration:

$$t_4 = V/A_a, \tag{39}$$

$$t_{12} = (1 - \upsilon)V/A_b + t_8 \tag{40}$$

The general model of the jerk pattern is suitable for both, the speed and the position control of the elevator which is defined by the landing factor υ (Fig. 6). Calculations Eq. (39) and Eq. (40) give the jerk pattern with intermediate zero periods. For the jerk pattern without an intermediate zero period time t_4 and time t_{12} must be calculated as:

$$t_4 = t_2 + t_a, \tag{41}$$

$$t_{12} = t_{10} + t_b \tag{42}$$

Time t_8 can be obtained only after derivation of the position function which is related to the speed function with $d(t) = \int v(t)dt$:

$$t_8 = t_a + t_2 + t_4 + \left(\frac{2}{\pi} - 1\right)t_b - \frac{V}{2A_b} - \frac{A_b}{2j_b} + \frac{L}{V} + \frac{j_a t_a^2 t_4 - j_a t_2^2 t_4 - A_a t_4^2}{2V} - \frac{2j_a t_a t_4 (t_2 + t_a)}{\pi V} \tag{43}$$

The model defined through Eqs. (34)-(43) must be expanded with criteria for the maximal permissible values of acceleration and deceleration:

$$A_{a\_\max} = \sqrt{\frac{2j_a V}{\sigma_a(\pi - 2) + 2}}, \tag{44}$$

$$A_{b\_\max} = \sqrt{\frac{2(1 - \upsilon)j_b V}{\sigma_b(\pi - 2) + 2}} \tag{45}$$

All parameters in Eqs. (35)-(43) are defined by the EMS design and they are constant for any ride of the elevator except the final position L. The time required for reaching the final position is $t_{\text{final}} = t_{12} + t_{10} - t_8 + t_b$.

5. The proposed anti-resonant and jerk free control scheme for an elevator mechatronic system

As it is described in Subsection 2.3, the IFOC control ensures the linear torque control and therefore the linear speed control of the EMS. Section 3 describes the causes and the nature of the phenomenon of oscillations and also proposes a solution for vibration suppression by band-stop filtering. The jerk control increases the comfort of passengers and protects the mechanical elements of the EMS (Section 4). Furthermore, the jerk control is a crucial factor in speed control which ensures a linear mode of speed controller. Owing to that, the linear PI controller is capable to have error free tracking of the speed reference (Subsection 2.4). As a result, a full anti-resonant and jerk limited control scheme is proposed and given in Fig. 13.

The input in the system is the desired position L^*. The speed trajectory generator (Subsection 4.2) generates the real time speed reference (V^*) for the PI speed controller. The PI controller (Fig. 7) calculates the difference between referent (V^*) and

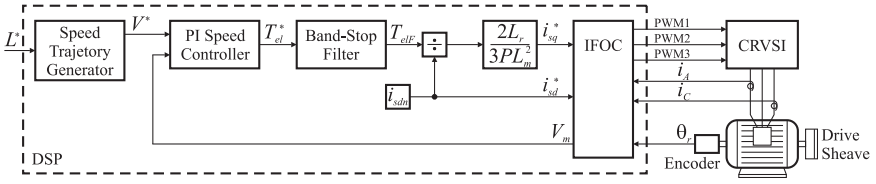

Fig. 13. The proposed anti-resonant and jerk limited control scheme for the elevator mechatronic system.

Table 1
The parameters of the mechanical subsystem of the EMS.

Parameters	Unit	Values
m_c, m_{cw}, m_{max}	kg	9.173, 15.151, 11.941
J_d, J_{o1}, J_{o2}	kgm^2	0.001435, 0.000133, 0.000133
r_d, r_{o1}, r_{o2}	m	0.0455, 0.052, 0.052
k_c, k_{cw}, k_{o1}, k_{o2}	N/m	97357, 950590, 72261, 72261
b_c, b_{cw}, b_{o1}, b_{o2}	Ns/m	21.4, 21.3, 29.7, 29.7
b_{cL}, b_{cwL}	Ns/m	8.3, 8.3

measured speed (V_m) and gives torque command T_{el}^* at the output. The drive torque reference is filtered by a band-stop filter (Subsection 3.2). The input parameter for calculating the quadrature current reference (i_{sq}^*) is the filtered torque command T_{elF}. The direct current reference (i_{sd}^*) is set to the nominal value, i_{sdn}. Both references of currents are inputs for the IFOC control (Fig. 5). The three PWM reference signals are fed to the CRVSI which supply the motor. The line currents (i_A and i_C,) and the rotor position are feedbacks from the power drive subsystem (Fig. 5).

6. Experimental results

According to the models described in Section 2, the scale down prototype of the EMS is constructed (Fig. 15). The EMS prototype preforms the proposed control scheme from Fig. 13. In this section the experimental results of proposed solutions described in Sections 3, 4 and 5 are presented.

6.1. The description of the EMS prototype

An overview of the EMS prototype is shown in Fig. 15a. The EMS prototype was developed at Department of Mechatronics at Faculty of Mechanical Engineering in Banja Luka. A control algorithm in the EMS prototype is implemented on floating point DSP TMS320C28335 from Texas Instruments. The processor is mounted on the Delfino F28335 controlCARD. The mother board for controlCARD is the TMS320C2000 Experimenter Kit (Fig. 15b). The main processor clock operates at 150 MHz. The software for code debugging and data monitoring is Code Composer Studio (CCS) version 5.3.0 (Fig. 15a). The connection between the PC and the DSP is realized via USB interface.

A measurement data are collected in the DSP memory. Using the CCS, measurement data are transferred through the USB interface to the PC and imported into the Matlab script where they are graphically represented.

The power drive subsystem is shown in Fig. 15c. The position sensor is an incremental encoder which has two channels and a maximum resolution of 14400 [imp/rev].

The parameters of the mechanical subsystem (model Eqs. (6)-(7)) are given in Table 1. Masses and radiuses are measured, inertias are calculated and parameters of the steel ropes are determined by identification. Other dimensions of the EMS prototype are shown in Fig. 14.

The values of all parameters which define the power drive subsystem (model Eqs. (14)-(15)) are given in Table 2.

The values of parameters which define the DSP control subsystem are given in Table 3. Controller parameters for the fast and aperiodic speed response are derived in [25]. The adapted derivation procedure for the EMS gives the equations for derivation of the optimal speed controller parameters as:

$$K_{Ps} = 0.4054\frac{J_m + J_{\text{load}}}{r_d \cdot \tau_{\text{speed}}}, \tag{46}$$

$$K_{Is} = 0.07024\frac{J_m + J_{\text{load}}}{r_d \cdot \tau_{\text{speed}}}, \tag{47}$$

where τ_{speed} is the sampling time of the speed control loop.

6.2. The experimental results of the proposed procedure for vibration suppression filter tuning

The PS and the GSS algorithms are executed in order to tune the proposed oscillation suppression filter. The experimental results are presented in Fig. 16. The process of searching the resonant frequency and the magnitude for that frequency is shown. The blue stems are the results of PS scanning of the EMS spectrum and the red stems are the results of the GSS algorithm. The additional frequency which is used in Eq. (32) is defined as 10% higher than the resonant frequency (the green stem in Fig. 16). The sampling frequency of the Goertzel algorithm is $f_{\text{Goertzel}} = 1/\tau_{\text{IFOC}}$ and τ_d=0.3 s.

The PS and the GSS algorithms obtain the resonant frequency in 14 steps: 7 steps in the PS algorithm and 7 steps in the

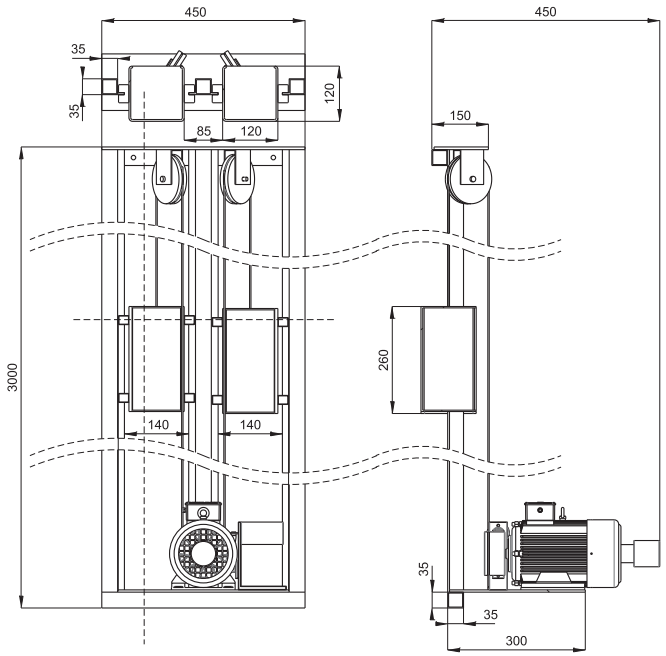

Fig. 14. Dimensions of mechanical structure of the EMS prototype.

Table 2
The parameters of the power drive subsystem of the EMS.

Parameters	Unit	Values
R_s, R_r	Ω	20, 9.3
L_s, L_r, L_m	H	0.7870212, 0.7388291, 0.7246325
J_m	kgm^2	0.0014
P		2
V_{DC}	V	325

Table 3
The parameters of the DSP control subsystem of the EMS.

Parameters	Unit	Values
K_{Pi}, K_{Ii}		183, 0.054
T_{max}	Nm	4
τ_{speed}	ms	10
τ_{IFOC}	ms	0.1

GSS algorithm (Fig. 16). Table 4 presents the results of the experiments which had a task to investigate the influence of the frequency step of the PS algorithm on the total number of iterations. Also, Table 4 shows the influence of the frequency step on the accuracy in determination of resonant frequency. Data from Table 4 are graphically presented in Fig. 17.

The error tolerance (ε) affects the accuracy of the final results by defining the number of iterations of the GSS algorithm. Band-stop filter parameters obtained by the experiments for different values of the error tolerance are shown in Table 5. For the same experiments and the same conditions the numbers of iterations are shown in Table 6 and graphically in Fig. 18.

The results from Table 5 were used to set up the band-stop filter. The resulting EMS magnitude characteristics are plotted using the data measured at the EMS prototype with a band-stop filter, Fig. 19.

The obtained parameters of the band-stop filter in the experiments with different loads of the EMS prototype are given in Table 7. All results are obtained using the same parameters: $T_{el}^{*}=4$ Nm, $\varepsilon=2$ and the frequency step is 10 Hz.

Fig. 19 shows the effect of the band stop filter, which is tuned by the proposed algorithm, on the frequency characteristic of the EMS. It can be seen that the desired result is achieved i.e. that the magnitude around resonant frequency is slightly

Fig. 15. The EMS prototype: a) the system overview, b) the power converter with the DSP and the interfaces, c) the induction motor with the incremental encoder and the drive sheave mounted on the shaft, d) the overhead sheaves.

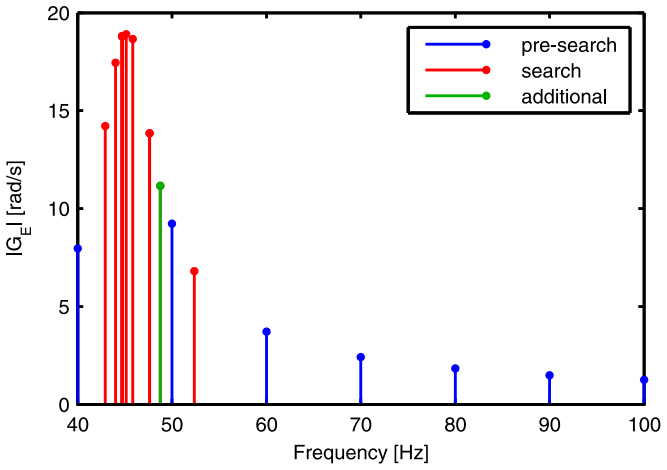

Fig. 16. The experimental results of the PS and the GSS algorithms for 50% load.

below zero. This means that in the time speed response there will not be the occurrence of damped oscillations at resonant frequency. Elimination of resonant frequency in the time speed response at step torque excitation (T_{el}^{*}) is shown in Fig. 20. Comparing speed responses in Fig. 2 and Fig. 20, the effectiveness of the proposed algorithm for filter tuning at all loads is obvious.

Fig. 20 shows speed response without the speed controller because the reference is torque T_{el}^{*}. When the speed (V^{*}) is a

reference, than the speed control is in operation. If proposed filtering is not used, the speed control is impossible, which is shown in Fig. 21. The same figure shows the significance and quality of the proposed control scheme (Fig. 13).

The developed algorithm does not depend on the load and could be performed without EMS parameters and measuring the mass in the elevator car (Table 7). It could be noticed that small deviations of the damping factors do not influence the overall EMS performance. The error tolerance influences the number of total iterations as well as accuracy. The error tolerance greater than 3 and less than 1 has no influence on accuracy (Fig. 19, Table 5), but influences the number of iterations (Table 6). The error tolerance between 1 and 3 is optimal regarding accuracy and the time required for the tuning process. The selection of the frequency step in the PS algorithm is not crucial for the algorithms performance at all. The larger frequency step means less iterations of the PS algorithm, but more iterations of the GSS algorithm and vice versa (Table 4). The total number of iterations is the same for all values of the frequency step. In all combinations presented in this section the EMS has the required vibration suppression.

Table 4
The number of algorithm iterations and the resonant frequency obtained for different PS frequency steps and $\varepsilon=2$.

PS step:		10	15	20	30
iteration	PS	7	6	5	4
	GSS	7	8	9	10
	total	14	14	14	14
f_0		45.15	45.21	45.24	45.02

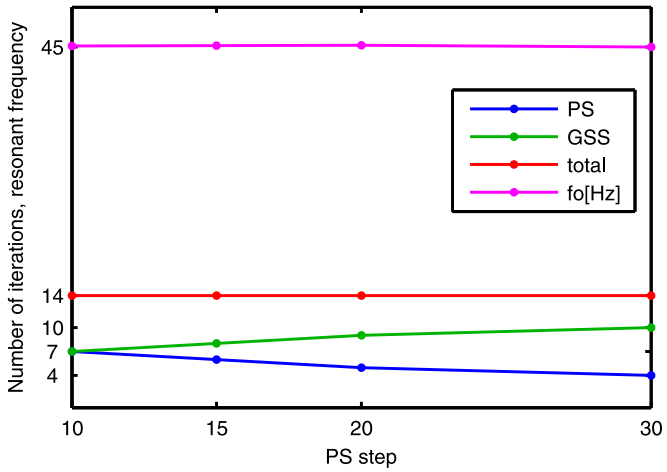

Fig. 17. The number of algorithm iterations and the resonant frequency against PS frequency steps for $\varepsilon=2$.

Table 5
The band-stop filter parameters (f_0, ς_Z and ς_P) for different error tolerance ε.

Parameter	$\varepsilon=0.05$, 0.1	$\varepsilon=0.5$, 1	$\varepsilon=2$	$\varepsilon=3$, 5, 10
f_0	44.96	44.98	45.15	44.72
ς_Z	0.063	0.062	0.056	0.074
ς_P	0.426	0.421	0.393	0.481

Table 6
The number of algorithm iterations for different error tolerance ε and 10 Hz PS frequency step.

ε:	0.05	0.1	0.5	1	2	3	5	10
PS	7	7	7	7	7	7	7	7
GSS	15	14	10	9	7	6	5	4
total	22	21	17	16	14	13	12	11

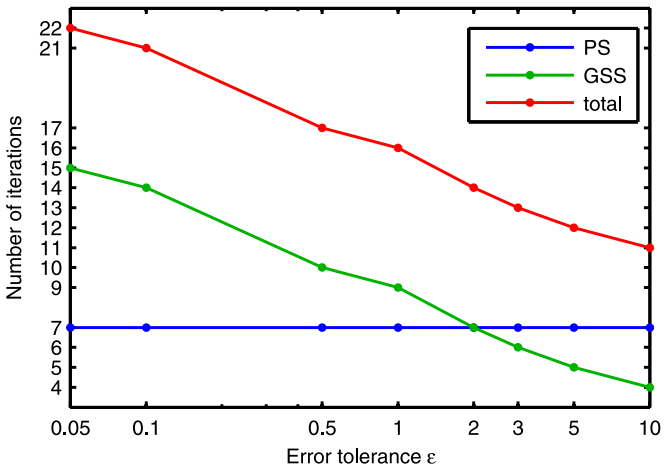

Fig. 18. The number of algorithm iterations for different error tolerance ε and 10 Hz PS frequency step.

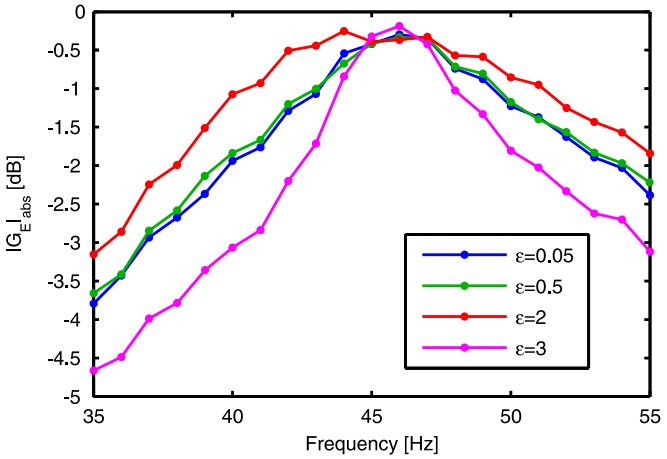

Fig. 19. The magnitude characteristics obtained by the experiments of the EMS prototype with a band-stop filter around the resonant frequency for different error tolerance and 50% load.

Table 7
The band-stop filter parameters (f_0, ς_Z and ς_P) for different elevator loads.

Parameter	0%	25%	50%	75%	100%
f_0	45.41	45.14	45.14	45.14	44.72
ς_Z	0.0566	0.0605	0.0563	0.0536	0.0655
ς_P	0.2906	0.3134	0.2928	0.2790	0.3411

6.3. *The experimental results of the proposed jerk free speed control*

Three characteristic shapes of the jerk function were used in the experiments. Fig. 22 shows the speed and the position errors of the speed controlled EMS. The EMS prototype (Fig. 15) is 50% loaded and the final destination is 2 m. The four cases were tested. The three cases of the jerk patterns without the intermediate zero periods are: sine ($\sigma = 1$), quasi-trapezoidal ($\sigma = 0.5$) and square ($\sigma = 0$). The fourth case is based on a similar speed trajectory (the same slope and the acceleration duration), but with the uncontrolled jerk.

The experimental results for the EMS prototype and different loads are shown in Fig. 23. For the three characteristic loads (0%, 50% and 100%) and the sine shape of the jerk, the quadrature current and the position are measured. The jerk pattern has adapted time of acceleration and deceleration. The adaptation of acceleration is used for the maximal motor utilization and for the linear mode operation of speed regulator. The measurements for the unadapted jerk are shown in Fig. 23, too.

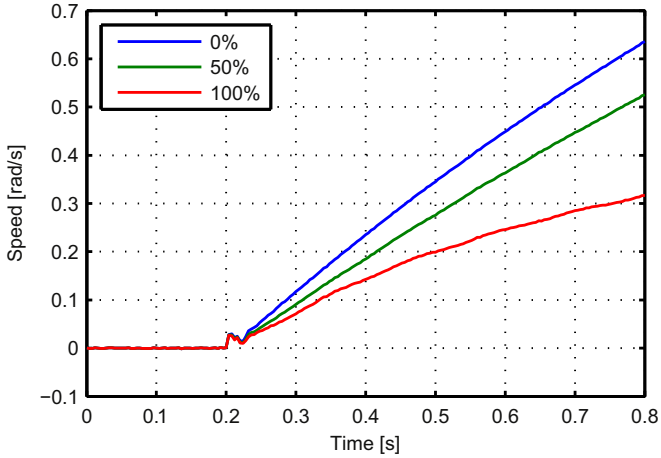

Fig. 20. The response of the EMS with proposed vibration suppression on the step torque reference and for different loads.

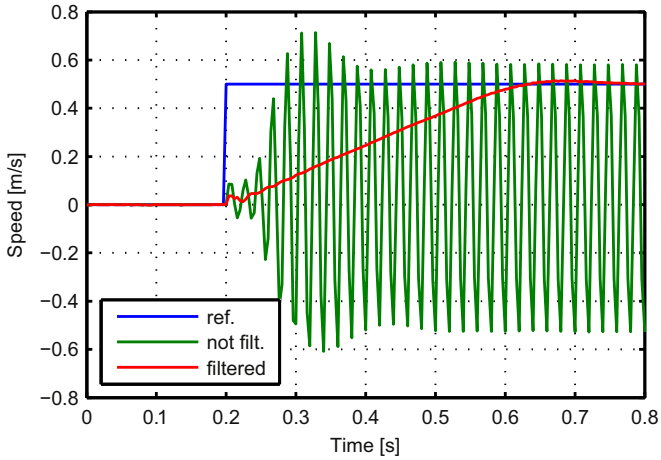

Fig. 21. The speed response of the EMS with and without proposed vibration suppression on the step speed reference.

If the jerk is controlled and limited to the permissible value, the position error of the speed controlled EMS is minimal or eliminated. The tracking position error and the final destination error are several times smaller than the errors with uncontrolled jerk pattern. The influence of the jerk shape on speed and position errors is negligible (Fig. 22). The adaptation of the jerk pattern according to Eqs. (37)-(40), Eq. (44) and Eq. (45) influences the ride time, especially at higher loads. The EMS with the unadapted jerk control needs more time for one ride as well as for loads greater than 50% (Fig. 23).

7. Conclusions

A new synergistic solution to the problem of vibration of the EMS is presented in this paper. Elimination of vibration is solved by software modifying speed controller and by introducing a new procedure for determining EMS resonant frequency. The proposed anti-resonant and jerk free control scheme for the EMS is a flexible and effective solution applicable on all EMS types without modifications to the hardware. The proposed algorithms were tested on DSP with floating point arithmetic, but with minimum corrections they can also be performed on processors with fixed point arithmetic.

Additional contribution of this paper is the proposed generalized model of speed reference generator that can be used to create almost any jerk pattern proposed in the literature. It is possible now to define all parameters of elevator car movement by only one speed reference generator and to compare different types and profiles of movement easily.

The conclusion of the research is that the smooth curve of speed reference with small slope is not a sufficient measure for suppressing resonant vibration. On the other hand, filtering the output signal of the speed controller is not also able to cancel vibration if the speed reference is defined by sudden changes in acceleration. It has been verified by experiments that only synergistic effect of controlling a jerk and filtrating the reference torque could eliminate vibrations caused by resonant frequencies.

Adequate band-stop filter adjustment is necessary in order to suppress vibrations with proposed synergistic solution. By

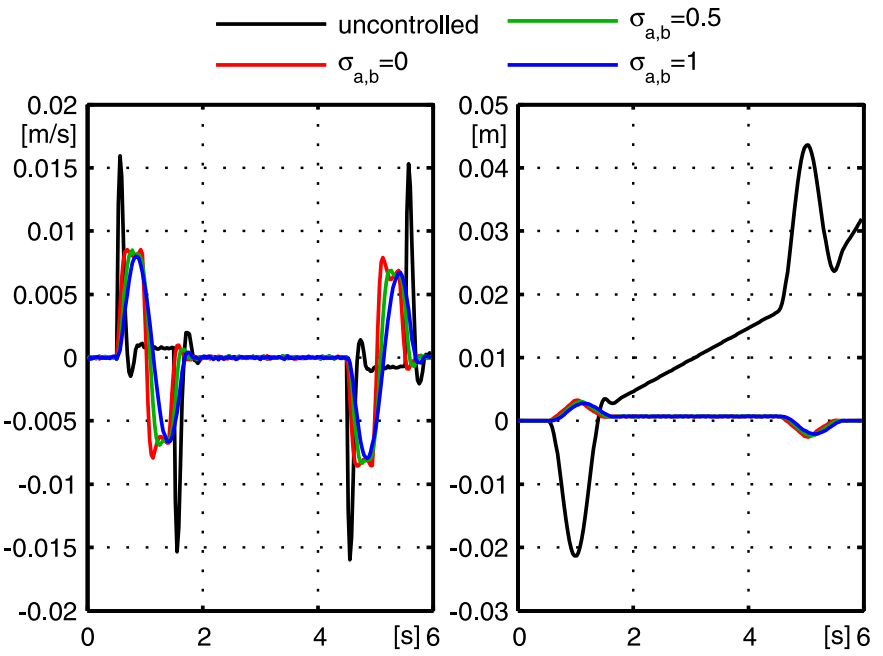

Fig. 22. The speed and the position errors obtained by the experiments on the EMS prototype and for different shape factors and the uncontrolled jerk.

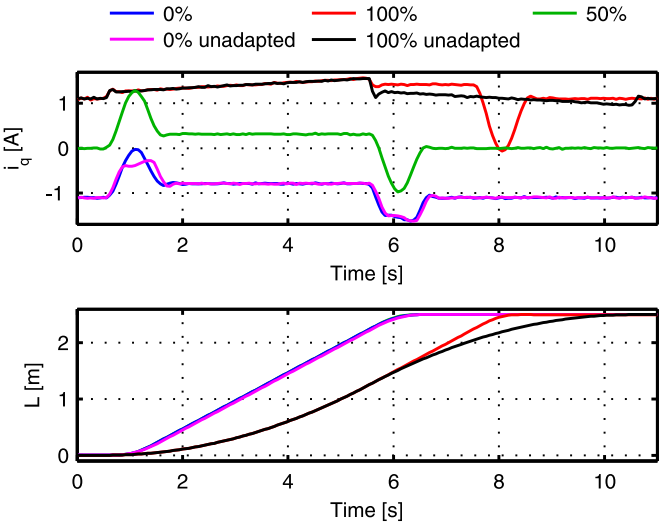

Fig. 23. The quadrature current and the position trajectories for different loads and the same jerk pattern.

computer simulations and experimental tests it has been proven that filter adjustment, by using the proposed procedure, based on the application of Goertzel algorithm and Kiefer search algorithm, is correct and can be easily applied. The algorithm program code is not computationally demanding and uses less than one quarter of process time required for IFOC.

The solution proposed in this paper can easily be implemented in EMS standard control units and it can be used as software improvement for all modern elevators. Also, the proposed solution for vibration suppression is model-independent so can be adapted and used in other similar systems.

References

[1] A. De Almeida, S. Hirzelb, C. Patrãoa, J. Fonga, E. Dütschkeb, Energy-efficient elevators and escalators in Europe: an analysis of energy efficiency potentials and policy measures, Energy Build. 47 (2012) 151–158.
[2] W.D. Zhu, Y. Chen, Theoretical and experimental investigation of elevator cable dynamics and control, Trans. ASME 128 (2006) 66–78.

[3] H. Li, Z. Gong, W. Lin, T. Lippa, Motion profile planning for reduced jerk and vibration residuals. in: Proceedings of SIMTech tech. repp. 32–37, 2007.
[4] M. Shreelakshmi, V. Agarwal, Jerk and loss minimization in electric elevator systems. In. Proceedings of CSCITA, 2014 International Conference onp. 19-23, 2014.
[5] G. Barney, L. Al-Sharif, Elevator Traffic Handbook, Theory and Practice, 2nd ed, Routledge, New York, 2016.
[6] A. Maccari, Vibration control by nonlocal feedback and jerk dynamics, Nonlinear Dyn. 63 (2011) 159–169.
[7] S.N. Vukosavić, M.R. Stojić, Suppression of Torsional Oscillations in a High-Performance Speed Servo Drive, IEEE Trans. Ind. Electron. 45 (1) (1998) 108–117.
[8] J. Bao, P. Zhang, C. Zhu, Computing Simulation and Dynamics Modeling of Flexible Hoisting Rope with Time-varying Length, J. Comput. Inf. Syst. 8 (10) (2012) 4177–4184.
[9] J. Vladić, R. Đokić, M. Kljajin, M. Karakašić, Modeling and simulations of elevator dynamic behavior, Tech. Gaz. 18 (3) (2011) 423–434.
[10] J. Bao, P. Zhang, C. Zhu, Modeling and control of longitudinal vibration on flexible hoisting systems with time-varying length, Procedia Eng. 15 (2011) 4521–4526.
[11] J. Petriková, Ľ. Ambriško, Determination of mechanical characteristics of single-wire rope loaded by tension using the videoextensometry, Int. J. Transp. Logist. 12 (2012) 25.
[12] D. Wang, D. Zhang, Z. Zhang, S. Ge, Effect of various kinematic parameters of mine hoist on fretting parameters of hoisting rope and a new fretting fatigue test apparatus of steel wires, Eng. Fail. Anal. 22 (2012) 92–112.
[13] J. Kang, S. Sul, Vertical-vibration control of elevator using estimated car acceleration feedback compensation, IEEE Trans. Ind. Electron. 47 (1) (2000) 91–99.
[14] A.C. Lecours, M. Otis, P. Belzile, C. Gosselin, A time-domain vibration observer and controller for physical human-robot interaction, Mechatronics 36 (2016) 45–53.
[15] A. Omiya, H. Inaba, H. Nagase, K. Miyoshi, T. Meguro, A Control Method for Reducing Vertical Vibration in a Long-stroke Elevators, Proc. of IPEC, , 1995, 458–463.
[16] Y. Yamazaki, M. Tomisawa, K. Okada, Y. Sugiyama, Vibration control of super-high-speed elevators, JSME Int. J. 40 (1) (1997) 74–81.
[17] D.H. Lee, J.H. Lee, J.W. Ahn, Mechanical vibration reduction control of two-mass permanent magnet synchronous motor using adaptive notch filter with fast Fourier transform analysis, IET Electr. Power Appl. 6 (7) (2012) 455–461.
[18] L. Biagiotti, C. Melchiorri, L. Moriello, Optimal trajectories for vibration reduction based on exponential filters, IEEE Trans. Control Syst. Technol. 24 (2) (2016) 609–622.
[19] C.M. Wang, W.C. Xiao, I.I.R. Second-order, Notch Filter Design and implementation of digital signal processing system, Proc. of ISCCCA, 13, , 2013, 576–578.
[20] C.I. Kang, C.H. Kim, An adaptive notch filter for suppressing mechanical resonance in high track density disk drives, Microsyst. Technol. 11 (2005) 638–652.
[21] S. Kaczmarczyk, W. Ostachowicz, Transient vibration phenomena in deep mine hoisting cables. Part 1: mathematical model, J. Sound Vib. 262 (2003) 219–244.
[22] S. Kaczmarczyk, W. Ostachowicz, Transient vibration phenomena in deep mine hoisting cables. Part 2: numerical simulation of the dynamic response, J. Sound Vib. 262 (2003) 245–289.
[23] E. Tartan, H. Erdem, A. Berkol, Optimization of Waiting and Journey Time in Group Elevator System Using Genetic Algorithm. in: Proceedings of IEEE INISTAp. 361-367, 2014.
[24] S.H. Sandilo, W.T. van Horssen, On variable length induced vibrations of a vertical string, J. Sound Vib. 333 (2014) 2432–2449.
[25] M.R. Stojić, S.N. Vukosavić, Design of Microprocessor-Based System for Positioning Servomechanism with Induction Motor, IEEE Trans. Ind. Electron. 38 (5) (1991) 369–378.
[26] J. Kiefer, Sequential minimax search for a maximum. in: Proceedings of the Am. Math. Socp.502-506, 1953.
[27] G. Goertzel, An algorithm for the evaluation of finite trigonometric series, Am. Math. Mon. 65 (1) (1958) 34–35.
[28] M.P. Shreelakshmi, V. Agarwal, Jerk and loss minimization in electric elevator systems, Proc. of IEEE Int. CSCITA, , 2014, 19–23.
[29] W.D. Zhu, L.J. Teppo, Design and analysis of a scaled model of a high-rise, high-speed elevator, J. Sound Vib. 264 (2003) 707–731.
[30] M.J.C. Ronde, M.G.E. Schneiders, Kikken EJGJ, van de Molengraft MJG, Steinbuch M. Model-based spatial feedforward for over-actuated motion systems, Mechatronics 24 (2014) 307–317.
[31] K.Y. Chen, M.S. Huang, R.F. Fung, Dynamic modelling and input-energy comparison for the elevator system, Appl. Math. Model. 38 (2014) 2037–2050.